PARAMETRIZATION OF TOPOGRAPHY FOR GROUND MOTION PREDICTION: SUMMARY AND FINDINGS

Manisha Rai and Adrian Rodriguez-Marek

Department of Civil and Environmental Engineering
Virginia Tech, Blacksburg, Virginia

Abstract

This paper summarizes our findings from a previous study on the effects of topography on ground motions. We analyzed the NGA-West2 dataset and proposed a model to predict topographic effects at a site. The model proposes modification factors for the expected amplifications or de-amplifications at a site, as a function of the relative elevation value at the site. As a part of this study, we also computed 2D topographic amplification at ground motion stations from simplistic numerical analyses and found that the logarithm of amplifications at stations, averaged over multiple orientations, were highly correlated with relative elevation value at the stations.

Introduction

Topography can significantly affect ground motions at sites located close to them (Bouchon, 1973; Boore et al., 1981; Bard, 1982). Typically, hills and ridges cause ground motion amplifications, whereas valleys and depressions cause de-amplification of ground motions compared to ground motions on a flat terrain (Davis and West, 1973; Rogers et al., 1974; Griffiths and Bollinger, 1979; Geli et al., 1988; Bouchon and Barker, 1996; Assimaki and Gazetas, 2004; Meunier et al., 2008; Rai et al. 2012; Maufroy et al., 2014; Rai et al. 2015). Topographically correlated damage patterns have been reported in a number of past earthquakes (Trifunac and Hudson, 1971; Celebi, 1987; Geli et al., 1988; Kawase and Aki, 1990; Hatzfeld et al., 1995; Bouchon and Barker, 1996). These effects however are not included in existing ground motion prediction equations. Consequently, there are no engineering tools to correctly estimate these effects at a site. In a previous study (Rai, 2015), we addressed this problem by proposing an empirical model to predict the effects of topography at a site. This paper presents a summary and important findings from that work.

Since topographic effects are systematically observed in the ground motions, they should also be predictable. Prediction of topographic effects can only be achieved by studying the dependence of the effects at a site on a family of topographic proxies or parameters. These proxies can then be used to predict the expected amplification/de-amplification at a given site. To develop topographic proxies for a given site, we employed two methods. In the first method, we used the elevation data around the site to compute geomorphometric parameters such as slopes, curvatures, and relative elevations and used them as topographic proxies for the sites. In the second method, we computed 2D topographic amplification at a given site from simple numerical analyses, and used the amplifications to develop a family of topographic parameters

for the sites. We used the NGA-West2 ground motion dataset, and computed topographic proxies from the two methods for each of the ground motion stations. We used the ground motion model residuals at those stations and tested if the residuals showed any trends with respect to one or more of the computed parameters. Statistical tests were performed to determine if the trends in the residuals with respect to the computed parameters were statistically significant. When the trends were found to be significant for a given parameter, we fit regression models to predict topographic effects as a function of that parameter. In the end, we compared different models to determine which model fitted the residuals most effectively. In the ensuing, we briefly cover the details of the analysis, and summarize our findings from that study. For a complete discussion, the readers are referred to Rai (2015).

Ground motion data

A subset of the NGA-West2 database used by Chiou and Youngs (2014) was used for the study. The subset consisted of ground motion recordings from 300 earthquakes of magnitude 3 and higher, at 3208 stations located in the regions of California, Alaska, Japan, Taiwan, China, Turkey, Italy, Iran, and New Zealand. As topographic effects are site effects, the residual component of interest for this study was the site residual, which represents the average error in

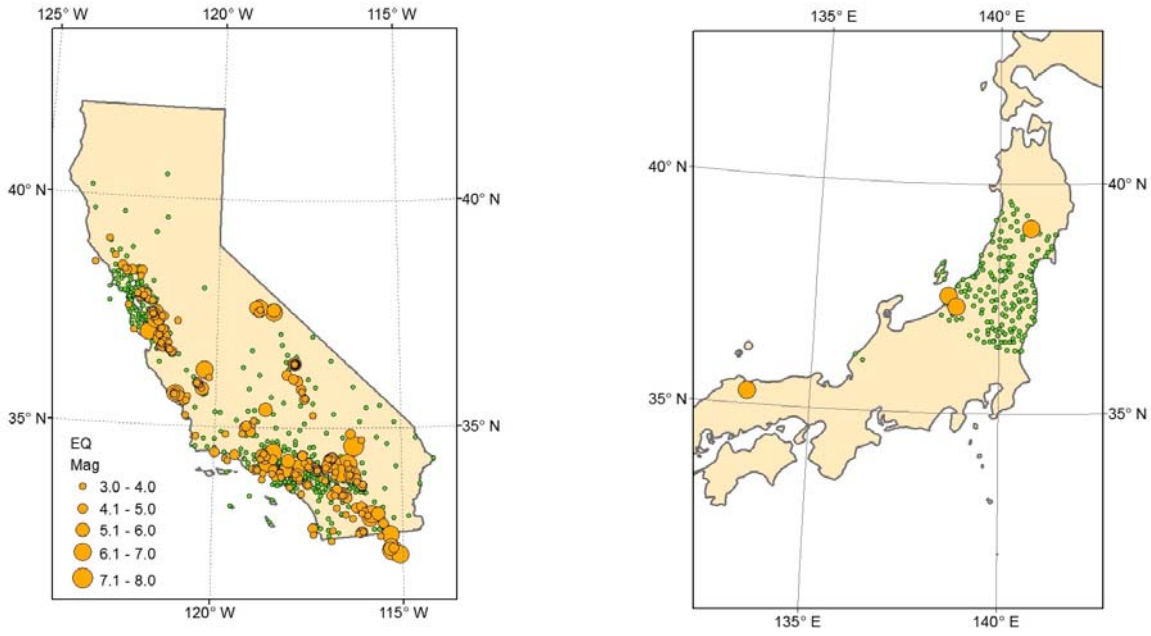

Figure 1. Locations of earthquake hypocenters (orange circles) and ground motion recording stations (green dots) for the data used in this study. Only stations with three or more recordings are considered. This filtering of data results in stations only within California and Japan.

prediction at a site, after removing the effects of earthquake. To obtain site residuals, the intra-event residuals (δW_{es}) from the Chiou and Youngs (2014) model were partitioned as follows:

$$\delta W_{es} = \delta S2S_s + \delta WS_{es} \quad (1)$$

where $\delta S2S_s$ are the site residuals, δWS_{es} are the site-and-event corrected residuals, and the subscripts *e* and *s* represent event and site, respectively. Each of the components of Equation 1 are assumed to be zero mean random variables with standard deviations ϕ, ϕ_{s2s}, and ϕ_{ss} for δW_{es}, $\delta S2S_s$ and δWS_{es}, respectively. To get stable estimates of site residuals at each station, we included those stations that had three or more earthquake recording on them. This constraint resulted in a total of 9,195 ground motions at 798 stations, located in California and Japan (Figure 1). The dataset consisted of ground motion residuals at 105 spectral periods from 0.01 s to 10 s.

Topographic parameters

We used two methods to compute topographic parameters. In the first method, we used the elevation data around the ground motion stations, and the resulting parameters are referred to here as the "geometry-based" parameters. In the second method, we performed a series of numerical analyses, and used the results from the analysis to obtain topographic parameters at the ground motion stations. These parameters are referred to here as the "numerical-analyses-based" parameter. In the following, we present a brief overview of the two types of parameters.

Geometry-based parameters

These parameters were computed in ArcGIS (ESRI, 2011) using the elevation data at the ground motion stations. We computed three parameters for each station: smoothed slopes (S_d), smoothed curvature (C_d) and relative elevation (H_d), where d is the scale-parameter that defines the size of the neighborhood used to compute the parameters. *Slope* is defined as the first spatial derivative of elevation and quantifies the steepness of the earth's surface. *Curvature* is the second spatial derivative of a surface and quantifies the convexity/concavity of the surface. Curvature values are positive for convex feature such as a hill or a ridge, and are negative for concave feature such as a valley or a canyon. *Relative elevation* is the difference between the elevation at a point on the surface and the mean elevation in the neighborhood of the point. Relative elevations have been used in the past to delineate ridges, slopes, and valleys in watershed study (Guisan et al., 1999; Jones et al., 2000). We used several different values of d in the analysis to study the effect of scale on the parameter values (see Rai, 2015). Figure 2 and 3 show the variation in the values of these geometry-based parameters with scale d.

Numerical-analysis-based parameter

These parameters were based on the results of a series of simplistic 2D numerical analyses. The idea behind this parameterization was to compute estimates of 2D amplifications due to surface topography at the stations, and then use these amplifications as an input in a regression analysis to predict actual amplifications at the stations. To compute these parameters, we performed simplistic numerical analyses on FLAC (Itasca Consulting Group, 2005) for each

station in the dataset. For each of these analyses we used by used planar 2D meshes with simplified V_s profiles, elastic soil properties, transmitting boundary conditions, and sinusoidal input motions. The top surface of the mesh was fit to the shape of the cross-sectional profile of the surface at the station in a given orientation. As an example, Figure 4 shows the cross-

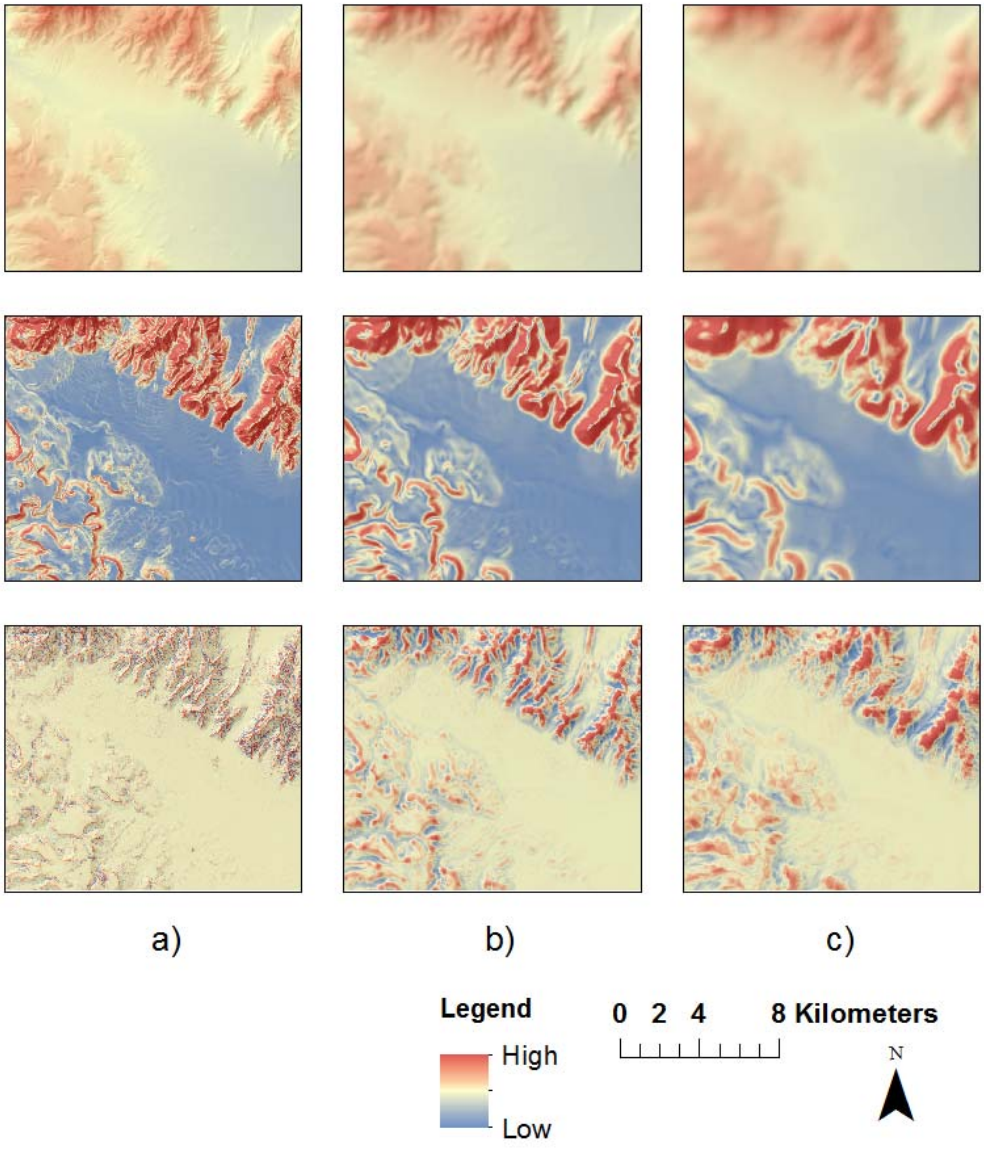

Figure 2. The top row consists of smoothed elevation raster, with a) no smoothing, b) smoothing using a scale (d) of 360 m, and c) smoothing using a scale of 720 m. The middle row shows corresponding smoothed slopes and the bottom row shows corresponding smoothed curvatures. Both smoothed slopes and curvatures are computed using corresponding smoothed elevations.

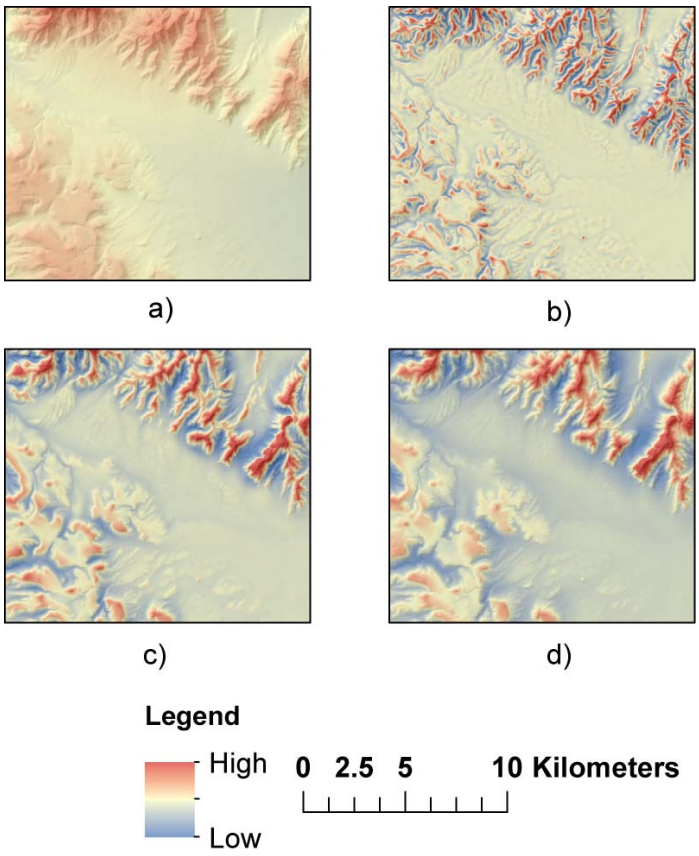

Figure 3. The variation of relative elevation with scale is shown. Shown are the a) elevation raster, b) H_{500}, c) H_{1500}, and d) H_{3000}. Note that at smaller scales, finer features are visible. As the scale is increased, the broader features become more prominent and finer details are lost.

sectional profiles that were computed for the Tamalpais peak station in California using the elevation data around the station in six orientations. This step was repeated for all the other stations in the dataset. A cosine tapered sinusoidal velocity was used as an input at the base of the mesh, and the resultant time history was recorded at the top surface of every mesh. Using the recorded motions at every station, and for every orientation, we computed the peak ground acceleration (PGA) at the station in six orientations. For each 2D analysis, we also performed a 1D analysis with no topography. The ratio of PGAs from the 2D and 1D analyses was computed. This ratio represents the value of amplification due to topography from the 2D analysis. A schematic illustration of the mesh and the applied boundary conditions are shown in Figure 5 for the Tamalpais peak stations for one of the orientations shown in Figure 4.

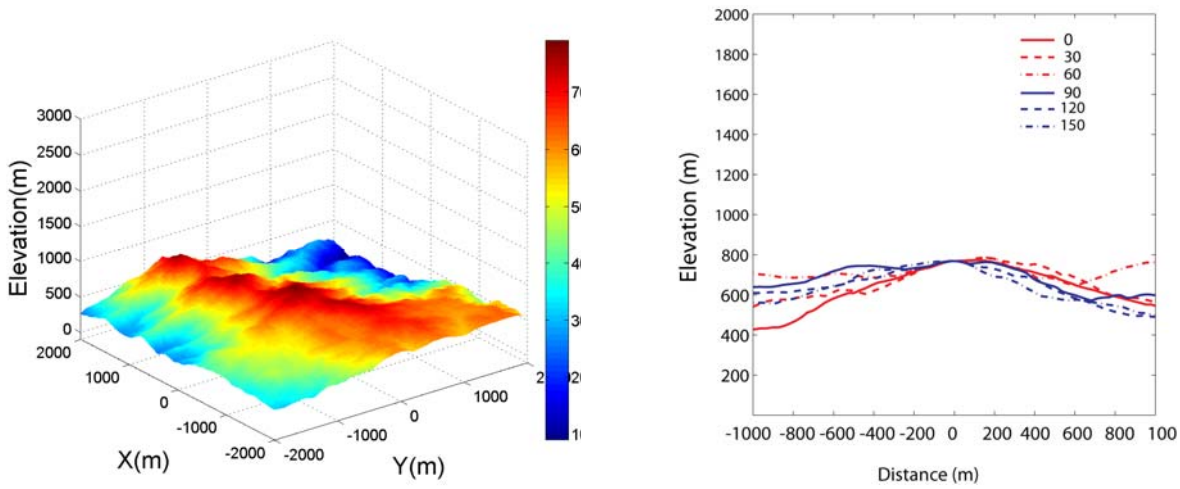

a) b)

Figure 4. 3D terrain around a site (left) and cross-sectional profiles across the station in 6 different directions (right) are shown for the Tamalpais peak B station (37.9231, -122.5983). The recording station is located at [0, 0] m.

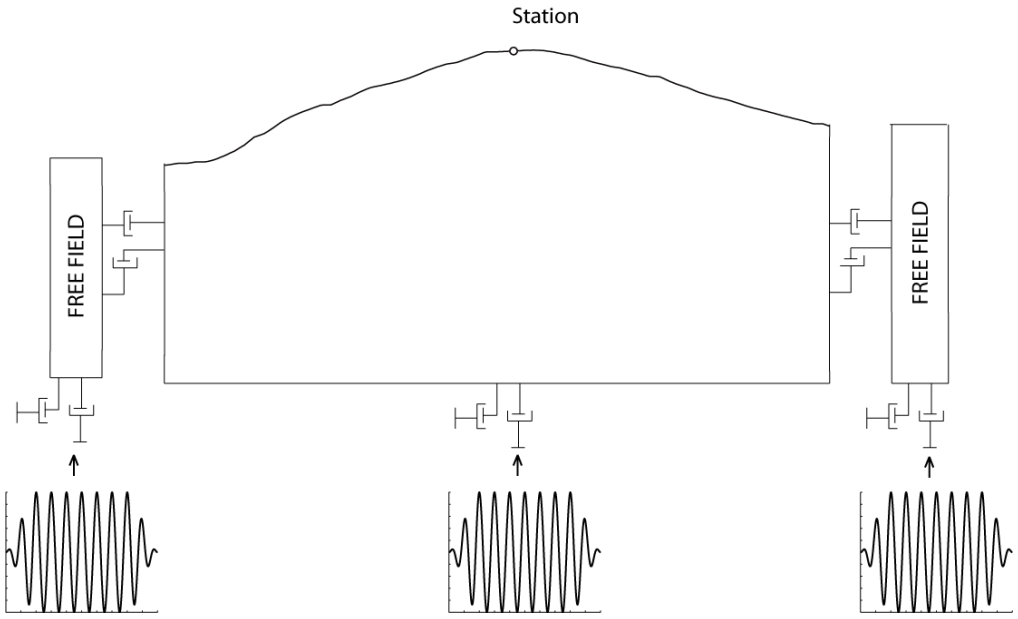

Figure 5. Schematic illustration of the finite difference model used for the analysis at one of the recording stations. The model uses a realistic topographic cross-section profile at the top. The station is located at the surface, equidistant from both the lateral edges. The height of the station from the base is the same for all stations. Free-field boundary conditions are applied to the lateral boundaries and quiet boundary conditions are applied at the base.

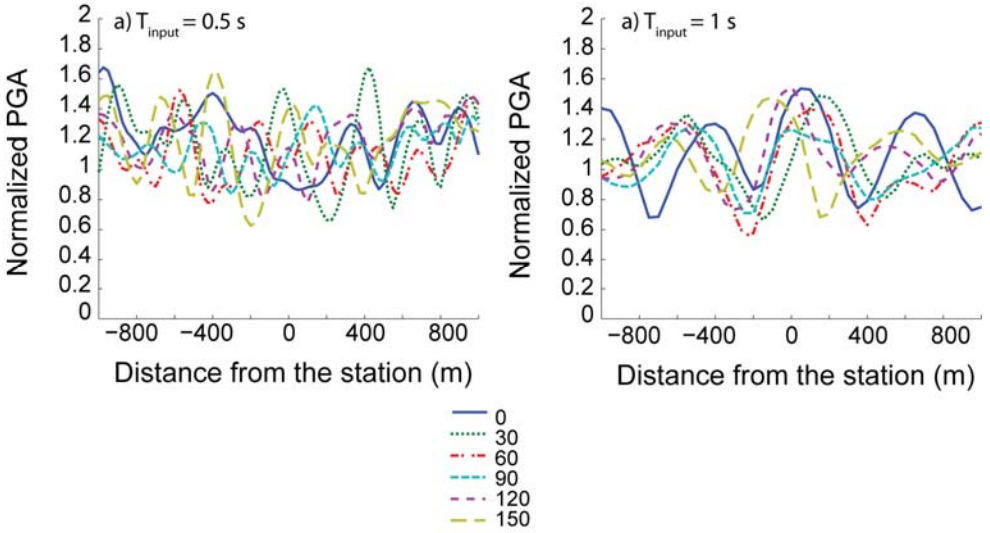

Figure 6. *Normalized PGA* values for the six cross-sections of the Tamalpais peak B station are shown for an input wave of period 0.5 s, and 1 s. The amplification and deamplification patterns seem to emerge at distances proportional to the wavelength of input motion. Also note that the normalized PGA values are greater than one for most of the azimuths, indicating an average amplification at the station.

Each of the six analysis for a given station resulted in a steady-state *Normalized PGAs* for that direction. The *Normalized PGAs* is referred to here as the ratio of the PGA from the 2D analysis to the PGA from the corresponding 1D analysis. Figure 6 shows the variation of *normalized PGA* at the surface of Tamalpais peak station for six orientations. A pattern of amplification and de-amplification emerges along the surface, and the distances over which these variations occurred were proportional to the wavelength of input motion. Using these *Normalized PGA* values, we computed the sets of parameters listed in Table 1.

Table 1. List of parameters computed from the numerical analyses.

Parameter	**Description**
$\ln Amp_{avg}$	Mean of the six *lnAmp* values
$\ln Amp_{min}$	Minimum of the six *lnAmp* values
$lnAmp_{max}$	Maximum of the six *lnAmp* values
$\ln Amp_{par}$	*lnAmp* value parallel to line joining recording station and hypocenter
$\ln Amp_{perp}$	*lnAmp* value perpendicular to line joining station and hypocenter

The term ln*Amp* in the table is used to define the natural logarithm of the *Normalized PGAs*. We used the natural logarithm of amplification as a parameter because the ground motion residuals are also in the units of natural logarithm of spectral accelerations, and we were using these parameters to model the trends in these residuals. To compute lnAmp_{par} and lnAmp_{perp}, we computed the angle of the line joining the station to the earthquake hypocenter. Using this angle, we selected one of the six azimuths where we obtained the cross-sections and selected the one that is closest to the computed angle, and assigned the corresponding *lnAmp* value in that direction to $lnAmp_{par}$. We repeated this process to obtain the $lnAmp_{perp}$, this time selecting the azimuth closest to the angle perpendicular to the computed angle. This process resulted in a total of 15 ln*Amp* parameters for each ground motion station. Using these parameters, and the previous geometry-based parameter, we studied the trends in the intra-event residuals from the Chiou and Youngs (2014) ground motion model to determine if one or more of these parameters can predict biases in the residuals.

Residual analysis and parameter selection

Figure 7 shows a scatterplot of the site residuals ($\delta S2S_s$) and the H_{1500} values at the station. The figure shows a positive trend in the site residuals with respect to H_{1500} for periods greater than 0.3 s. Similar trends were seen for other values of scale *d* used to compute H_d. A similar analysis of the scatterplot of site residuals and corresponding slopes showed no systematic trends. We therefore removed slope values from our analysis.

We tested the statistical significance of the trends in the site residuals with respect to the relative elevation parameter H_d by first dividing the stations into three classes based on the value of the topographic parameter H_d and then testing if the mean site residuals in each of the three classes are statistically different from each other. To do this, we denoted the group of stations with $H_d > t\sigma_{H_d}$ as '*High*', the group with $H_d < -t\sigma_{H_d}$ as '*Low*', and the group with $-t\sigma_{H_d} < H_d < t\sigma_{H_d}$ as '*Intermediate*'. Here, *t* is a constant threshold and was used to set the class boundaries and σ_{H_d} is the standard deviation of H_d values at the stations in the dataset used in the study. We used t values of 0.5 and 1 to determine the effect of changing threshold on the classification and on the mean site residuals within each class. Note that this classification depended on the value of *d* (used to compute mean elevation), and t (used to set the class boundaries). As we had selected 3 values of *d* and 2 values of *t*, there were a total of 6 *d*-*t* combinations. Each of these *d*-*t* combinations resulted in a different classification.

After determining the topographic class for each ground-motion station for a particular combination of d and t, we used mixed-effects regression using Equation 1 on stations from a single class to compute class-specific ϕ_{s2s} and ϕ_{ss}, as well as the mean site residual ($\overline{\delta S2S_s}$), which is the average of the site residuals in that class. Regressions were conducted using the R package *lme4* (Bates et al. 2014). We repeated this process for stations in the other two classes and also for other combinations of d and t. The resultant $\overline{\delta S2S_s}$ values for the three classes are shown as a function of the spectral period for different combination of *d* and *t* (Figure 8). We can see that there is an intermediate period range (T = 0.2 s to T = 1.0 s) for which the $\overline{\delta S2S_s}$ value for the *high* class became greater than the $\overline{\delta S2S_s}$ value for the other two classes. Higher $\overline{\delta S2S_s}$ value implies that the recorded ground motions on the stations in that class were on average higher than predicted by the GMPE. The $\overline{\delta S2S_s}$ value for the *low* class typically reduces as

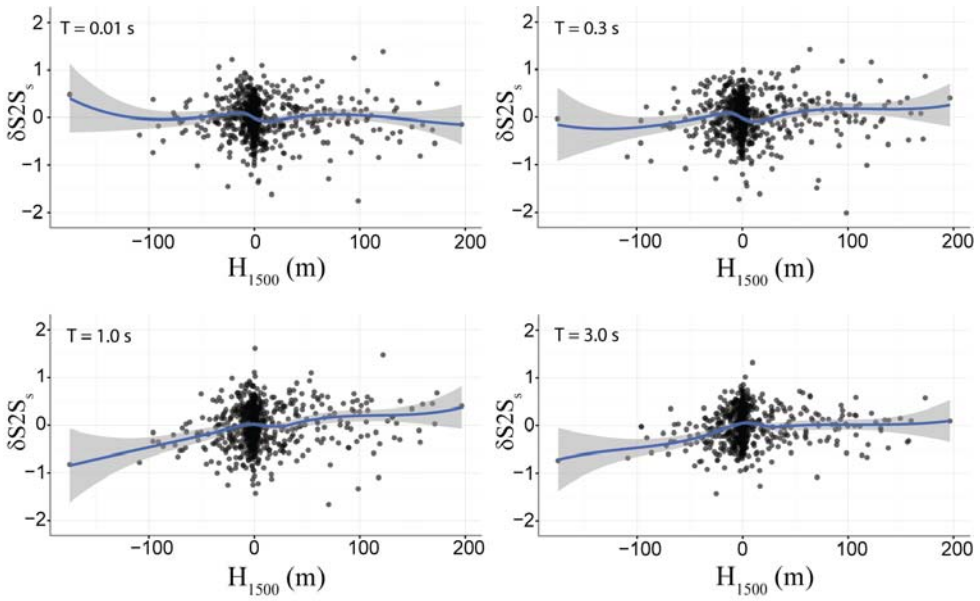

Figure 7. Site residuals ($\delta S2S_s$) from Equation 1 with relative elevation at a scale of 1500 m (H_{1500}). A moving average of the $\delta S2S_s$ terms computed using local regression (loess) is also shown.

period increases and becomes the lowest of the three classes for periods longer than 0.5 s. This means that at longer periods, the recorded motions in the *low* class were on average lower than the median predictions. As a majority of the stations in the dataset were classified as *intermediate* (e.g., 557 classified as *intermediate*, 103 as *low*, and 138 as *high,* for a scale of 1500 m, and t = 0.5), the $\overline{\delta S2S_s}$ value for the *intermediate* class can be expected to approximate the total $\overline{\delta S2S_s}$for the data. Thus, the $\overline{\delta S2S_s}$ value for the stations in the *intermediate* class was closer to zero compared to the other two classes. As the ground motions are presented in the log scale, the average amplification and de-amplification for each class were computed by taking the exponent of the observed $\overline{\delta S2S_s}$ for that class. After performing some statistical tests we selected a scale of 1500 m, and a threshold t of 0.5 for topographic classification.

We also compared the predictive abilities of the different numerical-analysis-based parameter. To do this comparison we fitted smoothed models to the intra-event residuals from the Chiou and Youngs (2014) GMPE by performing loess regression (Cleveland et al., 1992) as a function of each of the *lnAmp* parameters. For this regression, we used an α value of 1. α controls the degree of smoothing in the loess regression, with a value of 1 resulting in maximum smoothed function. We used this setting to avoid over-fitting the data. The coefficient of determination, or the R^2 values from these regressions are shown in Figure 9. Note that these R^2 values are of the order of 0.01, which seem to be rather small. These models are only accounting for a site-specific effect, thus we are only reducing a part of the total variance i.e. the site-specific variance. Other components of variability are still present in the residuals, even after removing the site-specific biases. Therefore the overall reduction in the variability of the intra-

event residual after the regression is small. Even though these R^2 values are small, they still provide information about the relative predictive abilities of individual *lnAmp* parameters. We can see in Figure 9 that out of the 5 *lnAmp* models, the $lnAmp_{avg}$ model has a relatively higher R^2 value on average. We therefore selected the $lnAmp_{avg}$ parameter from all the other *lnAmp* parameters for further analysis.

We compared the two types of shortlisted parameters, namely relative elevation and the $lnAmp_{avg}$ parameter and found that the two were very highly correlated linearly (Figure 10). The correlations between H_d and $lnAmp_{avg}$ reached a maximum when the value of d was equal to the wavelength of the input motion used to compute $lnAmp_{avg}$ (Figure 11). This is an important result as it shows that H_d was in essence modeling the average elastic 2D amplification of a wave with wavelength *d*. A similar observation was also made by Maufroy et al. (2014) who noted that the

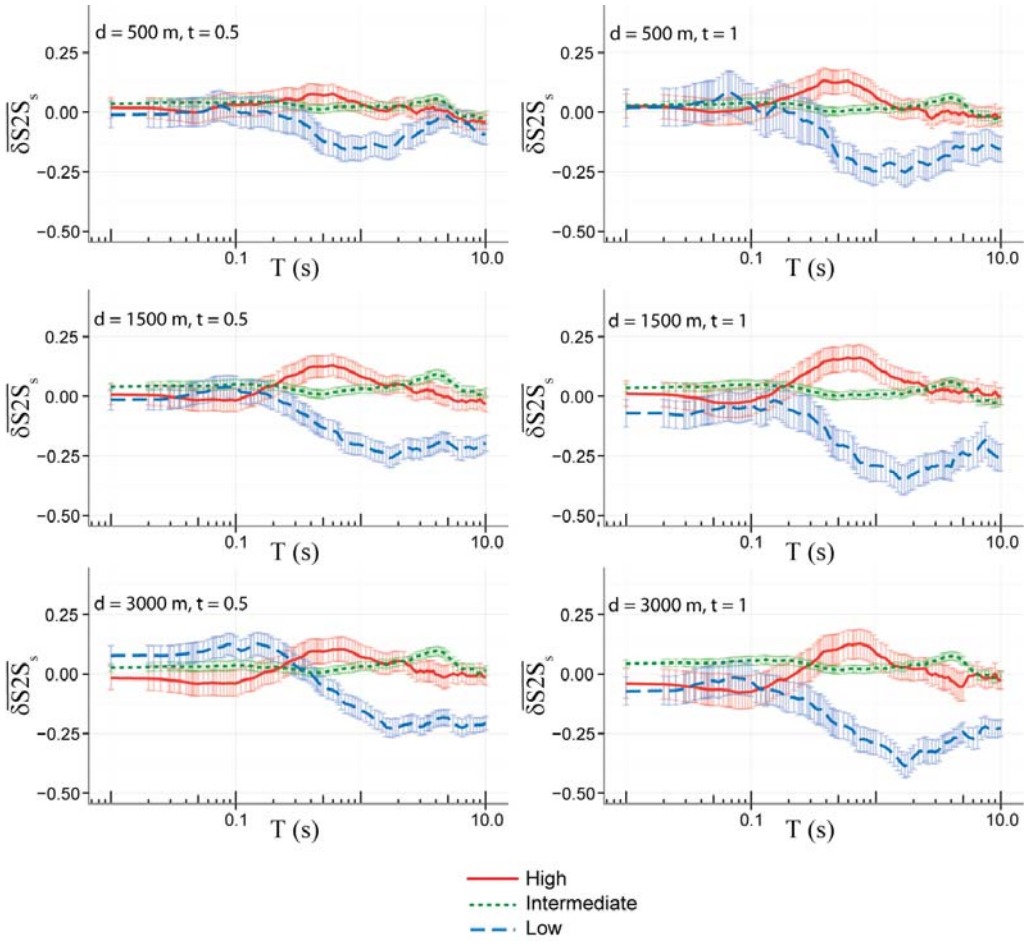

Figure 8. Mean site residuals ($\overline{\delta S2S_s}$) for the high, intermediate and low classes along with the +/- 1 standard deviation error bars.

amplifications at sites were highly correlated with the smoothed curvatures. However, this result also contrasts the findings from Burjánek et al (2014) who found that the amplifications at sites with pronounced topography are mostly controlled by the sub-surface shear wave velocities and not so much by the shape of the topographic feature.

The high correlation between H_d parameters, and the $lnAmp_{avg}$ parameters showed that the two parameters have similar information and they both captured topographic information. Thus they should have very similar predictive power, and we found that this was the case. Since computing the $lnAmp_{avg}$ parameters are expensive, and we are not gaining any additional reduction in the standard deviation in the fitted model, we used H_{1500} parameter for our final model.

Regression and model development

To account for the trends in ground motion residuals with respect to H_{1500} , we added a term containing the parameter to the right side of Equation 1, as follows:

$$\delta W_{es} = f(H_{1500}) + \delta S2S_s + \delta WS_{es} \qquad 2)$$

where δW_{es} is the intra-event residual from the Chiou and Youngs (2014) ground motion model, f is a function of the topographic parameter H_{1500}, $\delta S2S_s$ is the site residual after accounting for topographic effects, and δWS_{es} is the site-and-event corrected residual. We selected a multi-linear functional form for function f that has constant levels of spectral acceleration value for each topographic class with a linear transition from one class to the next class. The choice of this functional form was based on the fact that we observed distinct behavior within each class, as demonstrated by the different levels of mean site residuals. A multi-linear form proposes average levels of amplifications expected at sites within each class (e.g., high, low, or intermediate), and therefore it is much more robust in predictions than fitting say a linear model, that would predict increasing values of amplification for higher values of the topographic parameter, even though we did not have physical evidence to support such a model. The functional form we selected for accounting topographic effect is given by:

$$f = \begin{cases} c_{low} & H_{1500} < -20 \\ c_{int} & -17 < H_{1500} < 17 \\ c_{high} & H_{1500} > 20 \end{cases} \qquad 3)$$

with linear transition zones for intermediate values of H_{1500} (e.g., -20 to -17 or 17 to 20 m). In the model, we kept the transition zone from low/high class to intermediate class very steep such that the coefficient values can be more realistically constrained. The value of the coefficient c_{int} obtained from regression was fairly close to zero at all periods, and there was no reason to assume that they were different than zero. Because, we wanted to preserve the difference between different levels, we subtracted c_{int} from c_{high}, and c_{low} and smoothed out these values, ensuring that the c_{high}, c_{low} values gradually reached zero for periods where they were not significantly different than c_{int}. The updated values of coefficients c_{low}, c_{high}, ϕ_{ss}, and ϕ_{s2s} obtained through the mixed-effects regression on the full data set, and the epistemic uncertainties

(σ) associated with each coefficient, obtained from bootstrapping are reported in Table 2. These values can be added directly to the GMPE to estimate topographic effects at a site.

Table 2. Smoothed period dependent factors for f in Equation 3

Spectral Period (s)	c_{low}	$\sigma_{c_{low}}$	c_{high}	$\sigma_{c_{high}}$	ϕ_{s2s}	ϕ_{ss}
0.01	0	-	0	-	-	-
0.05	0	-	0	-	-	-
0.10	0	-	0	-	-	-
0.15	0	-	0	-	-	-
0.2	-0.0323	0.0263	0	-	0.4894	0.5518
0.25	-0.0573	0.0248	0.0293	0.0167	0.4704	0.5497
0.3	-0.0778	0.0255	0.0532	0.0175	0.4580	0.5428
0.4	-0.1100	0.0254	0.0910	0.0162	0.4396	0.5165
0.5	-0.1351	0.0226	0.1202	0.0158	0.4346	0.5060
0.75	-0.1805	0.0220	0.0851	0.0155	0.4335	0.4680
1	-0.2128	0.0219	0.0601	0.0142	0.4450	0.4460
1.5	-0.2583	0.0195	0.0250	0.0134	0.4309	0.4192
2	-0.2906	0.0192	0	-	0.4110	0.4054
3	-0.2906	0.0207	0	-	0.3854	0.3948
4	-0.2906	0.0213	0	-	0.3776	0.3830
5	-0.2764	0.0199	0	-	0.3772	0.3602
7.5	-0.2506	0.0236	0	-	0.3406	0.3483
10	-0.2323	0.0263	0	-	0.2802	0.3268

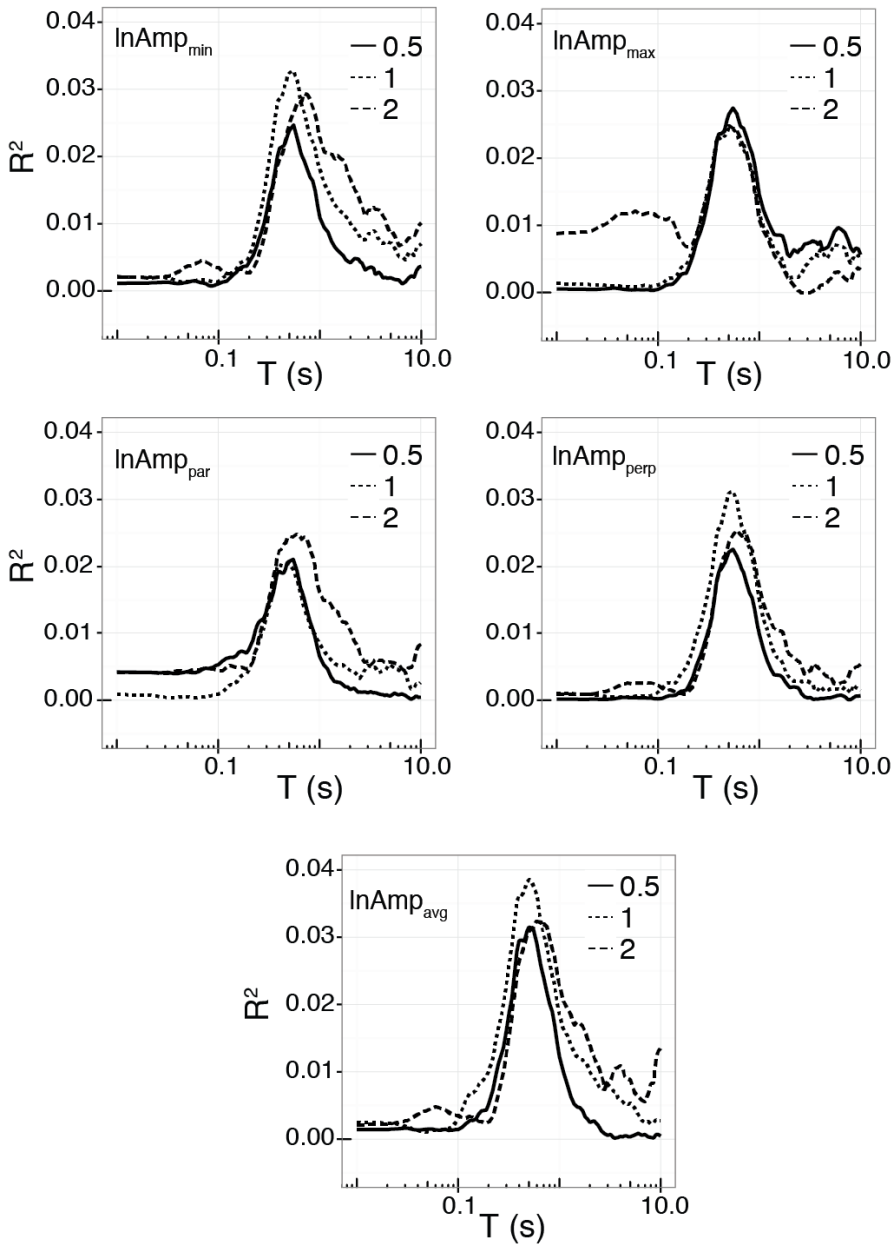

Figure 9. Coefficient of determination (R^2) value from the loess regressions on the intra-event residuals from the Chiou and Youngs (2014) model using the five *lnAmp*.

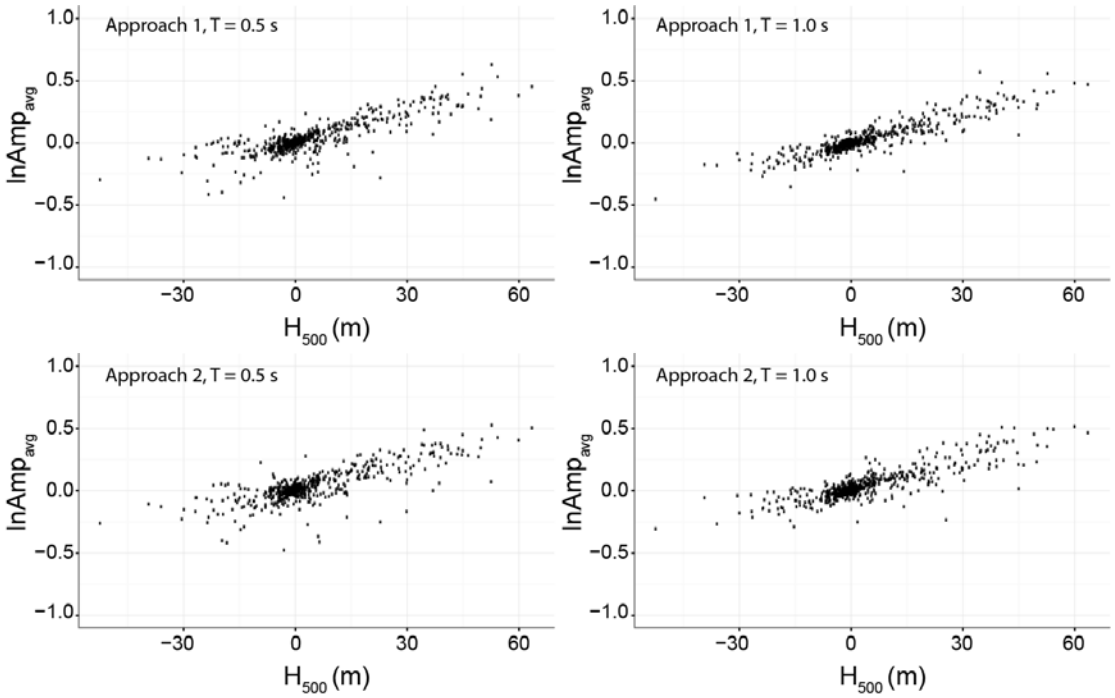

Figure 10. Scatterplot of the *lnAmp*$_{avg}$ obtained from the analysis using Approach 1 (constant V_s of 500 m/s for every station), and Approach 2 ($V_s = V_{s30}$), and the relative elevation parameter H_d for d values of 250 m - 3000 m. The values are shown for an input wave of period 0.5 s and 1 s.

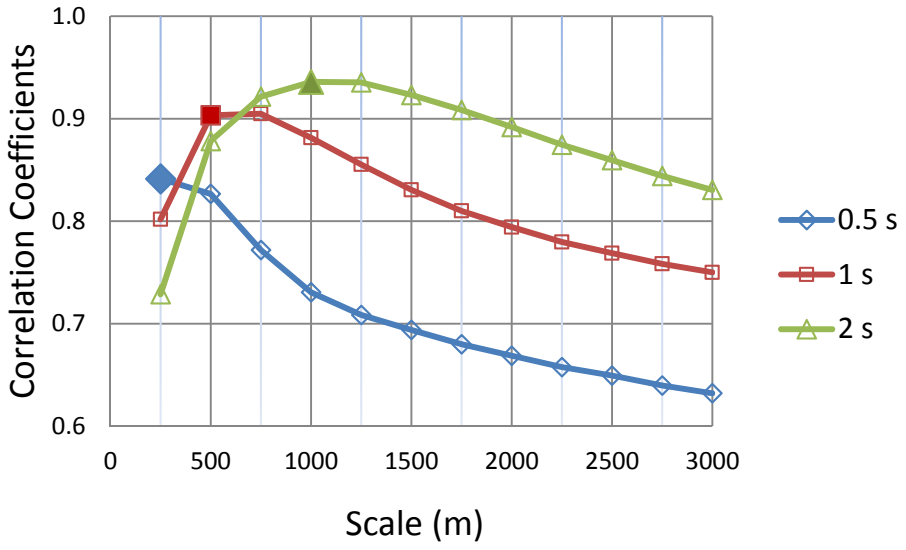

Figure 11. Correlation coefficient values between *lnAmp*$_{avg}$, and H_d for d values of 250 m - 3000. The three lines correspond to input wave of period 0.5 s, 1 s and 2s. The peaks are shown with solid symbols. Note that the respective peaks occur at a scale equal to the wavelength of the input motion.

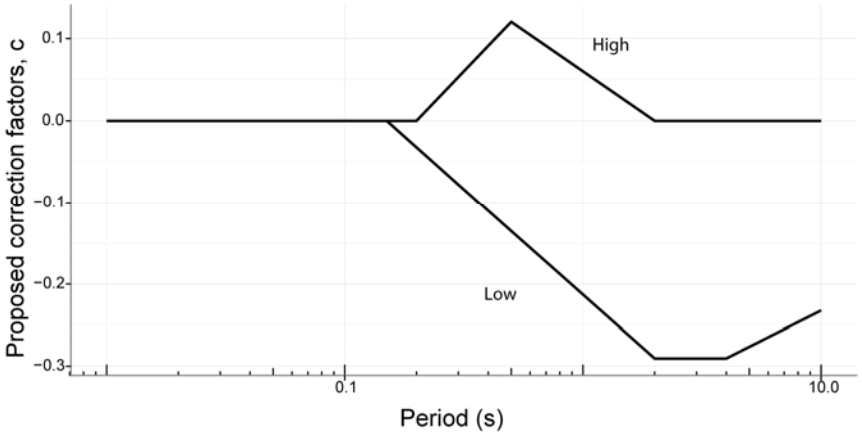

Figure 12. Proposed correction factors, c_{low} ($H_{1500} < -20$ m) and c_{high} ($H_{1500} > 20$ m) for topography. Linear interpolation should be used to estimate the correction factors for absolute H_{1500} values of 17 m – 20 m.

The *high* sites in the model showed a maximum amplification at a period of 0.5 s, and the *low* sites showed maximum deamplification between periods of 2 - 4 s. We could not establish the exact reason for this behavior; however we think that the majority of sites classified as *high* and *low* might be experiencing some sort of topographic resonance at these periods. Figure 12 shows the variation of the proposed correction factors for *high* and *low* class with period.

Conclusions

We used the NGA-West2 database to empirically study the effects of topography on earthquake ground motions. Topography was quantified using two types of parameters; the geometry-based parameters, and the numerical-analyses-based parameters. The three geometry-based topographic parameters that we studied were smoothed slope, smoothed curvature, and relative elevation. Two of these parameters, smoothed curvature and relative elevation, were highly correlated linearly. Of these two parameters, we only used relative elevation parameter for the regression analysis, as it a relatively simpler parameter to compute. The numerical-analysis-based parameters were computed using simplistic 2D numerical analyses. We computed approximate estimates of topographic amplifications at ground motion stations in multiple orientations, and used the natural logarithm of these amplifications to develop five other parameters at each station. We compared the predictive powers of these numerical-analyses-based parameters to determine the most efficient predictor of topographic effects. We finally selected $lnAmp_{avg}$ parameter, as it resulted in the highest R^2 value when a loess model was fit to the intra-event residuals with respect to each of the l*nAmp* parameters.

We compared the $lnAmp_{avg}$ values at the stations with the H_d values at the same stations and found that the two are highly correlated for several values of scale d. We found that for a given wavelength of input motion, the correlations between resulting $lnAmp_{avg}$ values and the H_d parameter reaches a maximum at a d value equal to the wavelength of input motion. This result

shows that the relative elevation parameter is modeling the elastic 2D amplification at the sites. Due to the high correlations between the $lnAmp_{avg}$ parameter and the H_d parameter, the two parameters carry very similar information, and also have similar predictive power. Using the ground motion residuals and the H_{1500} parameter, we fitted a model that predicts expected amplification or deamplification at a site as a function of H_{1500} at the site. The model proposes modification factors that can be used with an existing ground motion model. The proposed approach for computing topographic effects that is of using simplified numerical models to obtain parameters that can be used in regression analyses can also be used for capturing other effects of site amplification.

References

Assimaki, D., and Gazetas, G. (2004). "Soil and topographic amplification on canyon banks and the 1999 Athens earthquake." *Journal of earthquake engineering*, 8(01), 1–43.

Bard, P.-Y. (1982). "Diffracted waves and displacement field over two-dimensional elevated topographies." Geophysical Journal International, 71(3), 731–760.

Bates, D., Maechler, M., Bolker, B., and Walker, S., 2014. *lme4: Linear mixed-effects models using Eigen and S4*. R package version 1.1-7, http://CRAN.R-project.org/package=lme4.

Boore, D. M., Harmsen, S. C., and Harding, S. T. (1981). "Wave scattering from a step change in surface topography." *Bulletin of the Seismological Society of America*, 71(1), 117–125.

Bouchon, M. (1973). "Effect of topography on surface motion." *Bulletin of the Seismological Society of America*, 63(2), 615–632.

Bouchon, M., and Barker, J. S. (1996). "Seismic response of a hill: the example of Tarzana, California." Bulletin of the Seismological Society of America, 86(1A), 66–72.

Burjánek, J., Edwards, B., & Fäh, D. (2014). "Empirical evidence of local seismic effects at sites with pronounced topography: A systematic approach." Geophysical Journal International, ggu014.

Celebi, M. (1987). "Topographical and geological amplifications determined from strong-motion and aftershock records of the 3 March 1985 Chile earthquake." Bulletin of the Seismological Society of America, 77(4), 1147–1167.

Chiou, B. S. -J., and Youngs, R. R., 2014. Update of the Chiou and Youngs NGA Model for the Average Horizontal Component of Peak Ground Motion and Response Spectra, Earthquake Spectra, 30(3), 1117-1153.

Cleveland, W. S., E. Grosse, and W. M. Shyu (1992). Local regression models. Statistical models in S, 309–376.

Davis, L. L., and West, L. R. (1973). "Observed effects of topography on ground motion." *Bulletin of the Seismological Society of America*, 63(1), 283–298.

ESRI (2011). "ArcGIS Desktop: Release 10." Redlands, CA.

Geli, L., Bard, P.-Y., and Jullien, B. (1988). "The effect of topography on earthquake ground motion: a review and new results." *Bulletin of the Seismological Society of America*, 78(1), 42–63.

Griffiths, D. W., and Bollinger, G. A. (1979). "The effect of Appalachian Mountain topography on seismic waves." *Bulletin of the Seismological Society of* America, 69(4), 1081–1105.

Guisan, A., Weiss, S. B., & Weiss, A. D. (1999). "GLM versus CCA spatial modeling of plant species distribution." *Plant Ecology*, 143(1), 107-122.

Jones, K. B., Heggem, D. T., Wade, T. G., Neale, A. C., Ebert, D. W., Nash, M. S., Mehaffey, M. H., Goodman, I. A., Hermann, K. A., Selle, A. R., Bolgrien, D., Augustine, S., Pedersen, J., Lin, C. J., Viger, J. M., Chiang, D., Zhong, Y., Baker, J., and Remortel, R. D. V., 2000. Assessing Landscape Condition Relative to Water Resources in the Western United States: A Strategic Approach." Monitoring Ecological Condition in the Western United States, S. S. Sandhu, B. D. Melzian, E. R. Long, W. G. Whitford, and B. T. Walton, eds., Springer Netherlands, 227–245.

Hatzfeld, D., Nord, J., Paul, A., Guiguet, R., Briole, P., Ruegg, J.-C., Cattin, R., Armijo, R., Meyer, B., Hubert, A., Bernard, P., Makropoulos, K., Karakostas, V., Papaioannou, C., Papanastassiou, D., and Veis, G. (1995). "The Kozani-Grevena (Greece) Earthquake of May 13, 1995, Ms = 6.6. Preliminary Results of a Field Multidisciplinary Survey." *Seismological Research Letters*, 66(6), 61–70.

Itasca Consulting Group, Inc. (2005). "FLAC: fast lagrangian analysis of continua. User's manual"

Maufroy, E., Cruz-Atienza, V., Cotton, F., and Gaffet, S. (2014). "Frequency-scaled curvature as a proxy for topographic site-effect amplification and ground motion variability." *Bulletin of Seismological Society of America.*

Meunier, P., Hovius, N., and Haines, J. A. (2008). "Topographic site effects and the location of earthquake induced landslides." *Earth and Planetary Science Letters*, 275(3-4), 221–232.

Rai, M., Rodriguez-Marek, A., and Yong, A. (2012). "Topographic effects in strong ground motion." *Proceedings of the 15th World Conference on Earthquake Engineering, Lisbon, Portugal*, paper number 3843

Rai, M., Rodriguez-Marek, A., and Yong, A. (2015). "An empirical model to predict topographic effects in strong ground motion: Study using California small to medium magnitude earthquake database." *Earthquake spectra, In press*

Rai, M (2015). "Topographic effects in strong ground motion." Ph.D. dissertation, Virginia tech.

Rogers, A. M., Katz, L. J., and Bennett, T. J. (1974). "Topographic effects on ground motion for incident P waves: A model study." *Bulletin of the Seismological Society of America*, 64(2), 437–456.

Trifunac, M. D., and Hudson, D. E. (1971). "Analysis of the Pacoima dam accelerogram—San Fernando, California, earthquake of 1971." *Bulletin of the Seismological Society of America*, 61(5), 1393–1411.